ChemPlusChem

A Multidisciplinary Journal Centering on Chemistry

Chemistry Europe

European Chemical Societies Publishing

# Accepted Article

**Title:** Self-Assembly and Biorecognition of a Spirohydantoin derived from α-Tetralone: Interplay between Chirality and Intermolecular Interactions

**Authors:** Anita M. Lazić, Ivana S. Đorđević, Lidija D. Radovanović, Dragan M. Popović, Jelena R. Rogan, Goran V. Janjić, and Nemanja P. Trišović



**To be cited as:** *ChemPlusChem* 10.1002/cplu.202000273

**Link to VoR:** https://doi.org/10.1002/cplu.202000273

WILEY-VCH

# Self-Assembly and Biorecognition of a Spirohydantoin derived from α-Tetralone: Interplay between Chirality and Intermolecular Interactions

Anita M. Lazić,*[a] Ivana S. Đorđević,*[b] Lidija D. Radovanović,[a] Dragan M. Popović,[b] Jelena R. Rogan,[c] Goran V. Janjić,[b] and Nemanja P. Trišović [c]

[a] Dr. A. M. Lazić, Dr. L. D. Radovanović
Innovation Center, Faculty of Technology and Metallurgy
Karnegijeva 4, 11120 Belgrade, Serbia
E-mail: alazic@tmf.bg.ac.rs
[b] Dr. I. S. Đorđević, Dr. D. M. Popović, Dr. G. V. Janjić
Department of Chemistry-Theoretical chemistry and molecular modeling
Institute of Chemistry, Technology and Metallurgy, National Institute, University of Belgrade
Njegoševa 12, 11000 Belgrade, Serbia
E-mail: ivana.djordjevic@ihtm.bg.ac.rs
[c] Prof. J. R. Rogan, Dr. N. P. Trišović
Department of General and Inorganic Chemistry; Department of Organic Chemistry
Faculty of Technology and Metallurgy, University of Belgrade
Karnegijeva 4, 11120 Belgrade, Serbia

Supporting information for this article is given via a link at the end of the document.

**Abstract:** A racemic spirohydantoin derivative with two aromatic substituents, a tetralin and 4-methoxybenzyl unit, was synthesized and its crystal structure was determined. To define relationship between molecular stereochemistry and the spatial association modes, development of the crystal packing was analyzed through cooperativity of intermolecular interactions. Homo and heterochiral dimeric motifs were stabilized by intermolecular N–H···O, C–H···O, C–H···$\pi$ interactions and parallel interactions at large offsets (PILO), thus forming alternating double layers. The greatest contribution to the total stabilization came from a motif of opposite enantiomers linked by N–H···O bonds (interaction energy = –13.72 kcal/mol), followed by a homochiral motif where the 4-methoxybenzyl units allowed forming C–H···$\pi$, C–H···O interactions and PILO (interaction energy = –11.56 kcal/mol). The number of the contact fragments in the environment of the tetralin unit was larger, but the 4-methoxybenzyl unit provided greater contribution to the total stabilization. The statistical analysis of the data from the Cambridge Structural Database (CSD) showed that this is a general trend. The compound is a potential inhibitor of Kinase enzymes and AG protein-coupled receptors. A correlation between the docking study and the results of the CSD analysis can be drawn. Due to a greater flexibility, the 4-methoxybenzyl unit is more adaptable for interactions with the biological targets than the tetralin unit.

## Introduction

Chiral recognition plays an important role in natural systems. Within the crystal structures this phenomenon is reflected in prevalence of formation of the racemic crystals over conglomerates of the enantiopure ones from a racemic or scalemic solution.[1] Gavezzotti and Rizzato have suggested that this might be ascribed to longer persistency and/or faster propagation of the cohesive motifs which define the growth of racemic crystals.[1] Interestingly, they have also revealed that formation of racemic crystals is not necessarily advantageous, neither in terms of total crystal energies nor in the interaction energies of characteristic dimeric motifs in the crystal structure.

The biological effects of chiral compounds are achieved through the molecular recognition and chiral matching between the biological targets and the individual enantiomers. Namely, difference in affinity of the opposite enantiomers for a certain target results from their orientation in the recognition domain which further induces differences in modes of noncovalent interactions, especially hydrogen bonding.[2] In this context, it has recently been demonstrated that the structure and interaction propensities of molecules in their crystalline state can be used to screen them for binding compatibility with the targets.[3]

Hydantoin (imidazolidine-2,4-dione) represents a useful pharmacological scaffold which is incorporated into several marketed drugs, e.g. antiepileptics (phenytoin, mephenytoin, ethotoin), muscle relaxants (nitrofurantoin, dantrium) and androgen receptor antagonists (nilutamide, enzalutamide).[4] Namely, this scaffold has gained a reputation of a "promiscuous binder" due to its ability to interact with a variety of biological targets.[5] A comprehensive literature survey concerning this topic is not possible in the space devoted to the Introduction. Nevertheless, some significant biological targets and molecular mechanism underlying the functional responses will be described here.

Hydantoin-based antiepileptic agents block voltage-gated sodium channel through aromatic-aromatic interaction and N–H···aromatic bond.[6] Some hydantoin derivatives are tested *in vitro* for their 5-HT receptor affinities. Results of the molecular modeling studies and crystallographic analyses demonstrate

that the main ligand-receptor interactions between 5-phenyl-3-(2-hydroxy-3-(4-(2-ethoxyphenyl)piperazin-1-yl)propyl-5-methyl)hydantoin and 5-HT7R homology models involve a salt-bridge, C–H···$\pi$ interactions, $\pi$···$\pi$ stacking interactions and hydrogen bonds.[7] Yu *et al.* demonstrate that potent inhibitors of tumor necrosis factor-α converting enzyme with the hydantoin scaffold bind to the target protein *via* the amide nitrogen of hydantoin and the carbonyl oxygen creating a bidentate hydrogen bond.[8] A combination of structure-based virtual screening approach, enzymatic and cellular assays identify 5-benzylidenehydantoin as a new scaffold for the inhibition of the sirtuin protein activity.[9] These compounds exert the pharmacological activity through the formation of stacking interactions and van der Waals contacts. The hydantoin scaffold is placed in a niche defined by the four amino acid (AA) residues, while the phenyl unit participates in hydrophobic contacts with some of them.

Taking into the consideration these findings, we present the synthesis and characterization of a racemic spirohydantoin derivative bearing two aromatic substituents, namely a tetralin and 4-methoxybenzyl group (Figure 1). This compound contains one stereogenic center (the spiro atom) and its chirality is coupled with the helicity of the tetralin ring system. The main focus is oriented towards elucidation of the ability of this molecule to establish interactions with its environment in the crystal packing and with the potential biological targets. To define relationship between molecular stereochemistry and the spatial association modes, we analyze self-recognition within the crystal packing through interplay of intermolecular interactions with an emphasis on the contribution of the individual structural fragments. The affinity of the investigated compound for a certain biological targets is also examined and the modes of potential pharmacological action are discussed. According to the available docking tools, the investigated compound is recognized as potential inhibitor of Kinase enzymes and AG protein-coupled receptors. The pharmacological potential assessment is complemented by predicting its ADMET properties and biological availability through application of different empirical rules and software packages.

## Results and Discussion

**Molecular structure.** The representative ORTEP diagram of (*S*)-3-(4-methoxybenzyl)-6,7-benzo-1,3-diazaspiro[4.5]decan-2,4-dione is presented in Figure 1b. Molecular geometry was similar to other spirohydantoins, the bond lengths and angles were in normal ranges (Table S1).[10] The tetralin moiety and 4-methoxybenzyl group were positioned on the opposite sides of the plane of the hydantoin ring, both being nearly perpendicular to this plane (the dihedral angles of 81.52(5) and 88.78(5)°, respectively). This can be ascribed to the crystal packing effects. The non-aromatic six-membered ring as a part of the tetralin ring system adopted the half chair conformation with the NH group positioned pseudoaxially. The values of the torsion angles, C5–C10–C9–C8, C10–C9–C8–C7 and C9–C8–C7–C6, in the non-aromatic fused ring slightly deviated from those for non-substituted tetralin (Table S1).[11]

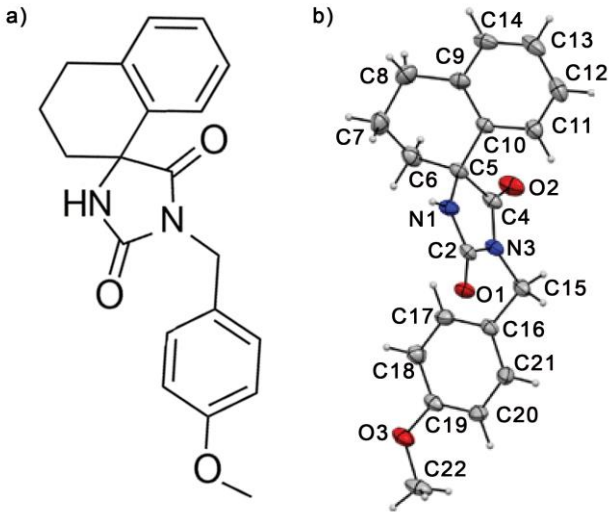


**Figure 1.** a) Chemical structure of 3-(4-methoxybenzyl)-6,7-benzo-1,3-diazaspiro[4.5]decan-2,4-dione; b) molecular structure of the (*S*)-enantiomer with atomic numbering scheme (hydrogen atoms are shown as small spheres of arbitrary radii). The thermal ellipsoids are plotted at the 30% probability level.

**Crystal packing and intermolecular interactions.** The studied compound crystallized in the monoclinic $P2_1/c$ space group. Each molecule was surrounded by ten neighboring ones, whereby their interactions can be described with seven dimeric motifs (Table 1). Interaction energy for each of them was calculated. Relative orientations of molecules, interaction energy and the type of intermolecular interactions are presented in Table 1. Of seven dimeric motifs, four were centrosymmetric (I–IV), while the other three did not have any element of symmetry. The main motif was the pair of opposite enantiomers linked by N–H···O hydrogen bonds in a head-to-tail fashion which generated an $R^2_2(8)$ ring (motif I, interaction energy = –13.72 kcal/mol). Together with motifs II, III and IV, this motif connected the molecules into the double layers with the tetralin and 4-methoxybenzyl units positioned at the double-layer surfaces (Figure 2). On the other side, along the *a*- and *b*-axis, motifs VI and VII joined the molecules in the single layer such that the 4-methoxybenzyl groups interdigitated between the neighboring tetralin ring systems. Heterochiral motif II was subject of a pair of C–H···O interactions between the tetralin methylene group and the carbonyl O2 atom which formed an $R^2_2(14)$ ring, (interaction energy = –8.18 kcal/mol). In homochiral motif III, the 4-methoxybenzyl groups were in close antiparallel contact allowing establishment of C–H···$\pi$ interaction, C–H···O interaction and parallel interactions at large offsets (PILO, interaction energy = –11.56 kcal/mol). Heterochiral motif IV contained only a pair of C–H···O interactions which resulted in formation of a centrosymmetric $R^2_2(8)$ ring (interaction energy = –2.52 kcal/mol). Homochiral motif VI involved C–H···O interactions, as well as, PILOs between two tetralin ring systems and two 4-methoxybenzyl groups (interaction energy of –8.59 kcal/mol). In homochiral motif VII, the molecules were linked through C–H···O interaction and C–H···$\pi$ interaction where the H atom of the methoxy group of one molecule was pointed at the phenyl group of the tetralin system of the neighboring one (interaction energy = –6.07 kcal/mol).

**Table 1.** Dimer motifs describing the types of intermolecular interactions observed in the crystal structure.

| Motif | | No[a] | Type of interactions | Strength of Interactions (kcal/mol) |
|---|---|---|---|---|
| I |  | 1 | Hydrogen bonds ($d$=2.12 Å) | –13.72 |
| II | 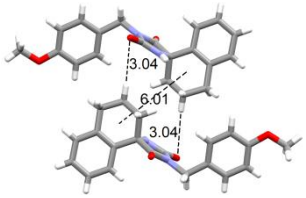 | 1 | C–H···O (3.04+3.04 Å) PILO (6.01 Å) | –8.18 |
| III | 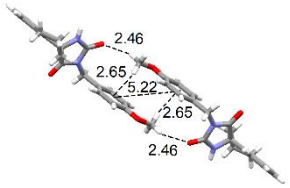 | 1 | C–H···$\pi$ (2.65 Å) PILO (5.22 Å) C–H···O (2.46 Å) | –11.56 |
| IV | 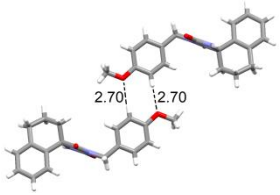 | 1 | C–H···O (2.70 Å) | –2.52 |
| V | 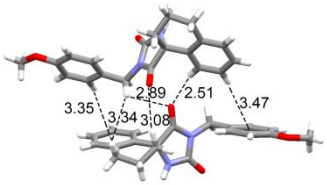 | 2 | C–H···$\pi$ (3.35+3.34+3.47 Å) C-H···O (2.89+3.08+2.51 Å) | –11.56 |
| VI | 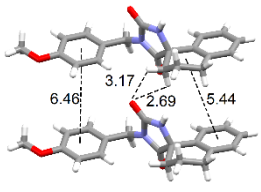 | 2 | C–H···O (2.69+3.17 Å) PILO (6.46+5.44 Å) | –8.59 |
| VII | 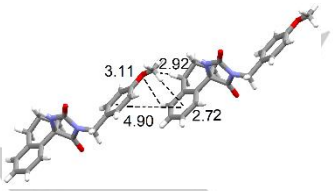 | 2 | C–H···$\pi$ (2.72 Å) C-H···O (2.92+3.11 Å) PILO (4.90 Å) | –6.07 |

[a] Number of the motifs wherein each molecule partook

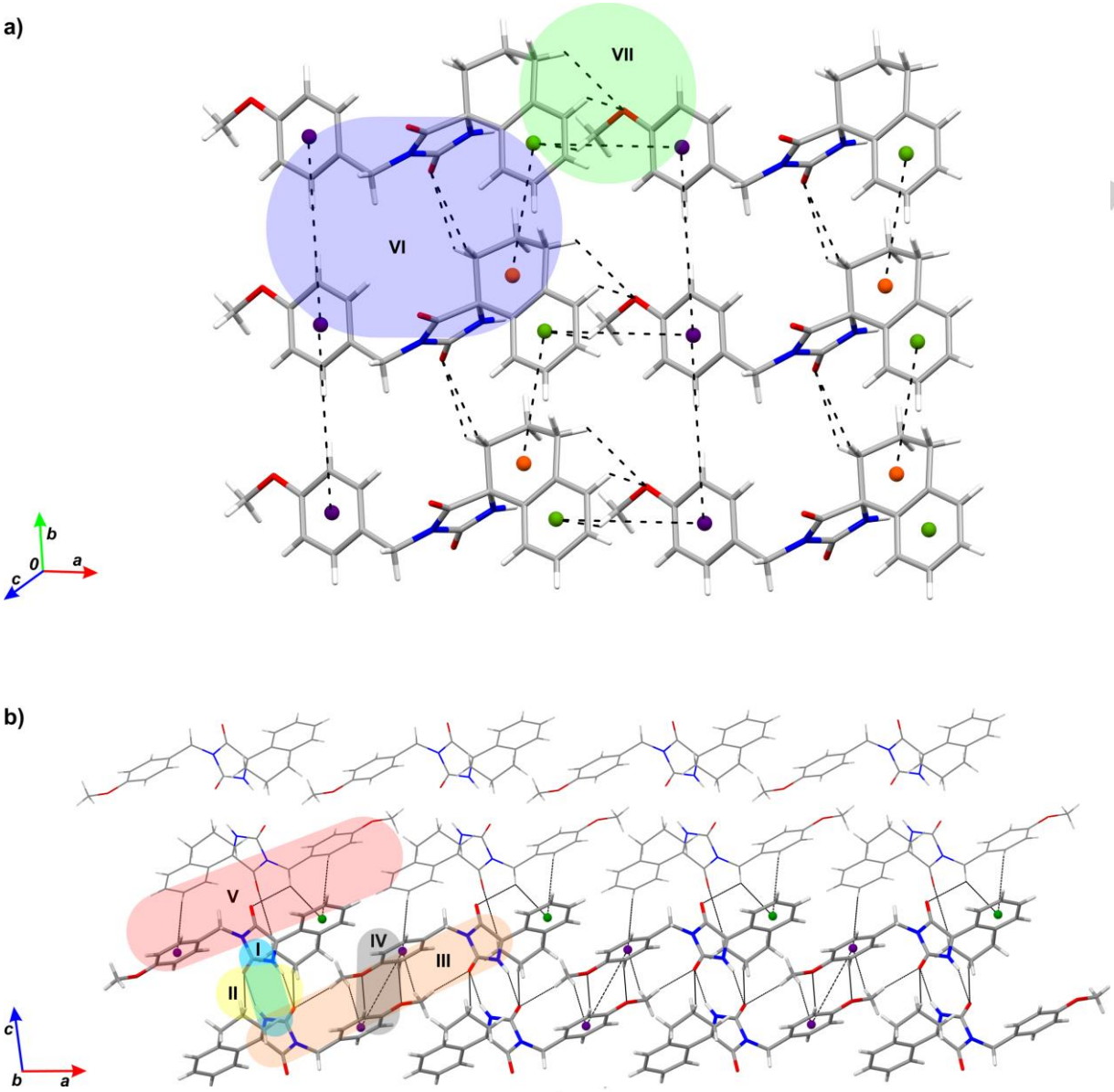


**Figure 2.** Presentation of the crystal packing of the investigated compound including the dimeric motifs associated with the presence of different intermolecular interactions: a) formation of the single layer through motifs VI i VII; b) formation of the double layer through motifs I, II, III and IV.

A hallmark structural feature of the investigated compound was alternation of double layers. Every double layer was similar to those above and below it, but the hydantoin rings of the adjacent double layers were positioned perpendicularly to each other. Connection between neighboring double layers was achieved only through homochiral motif V, whereby the association mode had two C–H···O and three C–H···$\pi$ interactions (interaction energy = –11.56 kcal/mol).

**Crystal packing and intermolecular interactions.** To better understand the interaction preference in the crystal packing of the studied compound, the statistical analysis of the particular interactions was applied. It revealed that C–H···O interactions were the most frequent (11 interactions), followed by C–H···$\pi$ (7 interactions) and PILOs (5 interactions), while the N–H···O hydrogen bonds were the smallest in number (2 interactions). Namely, a quantum-chemical study coupled with the statistical analysis of the crystal structures from the Cambridge Structural Database (CSD)[12] revealed that the benzene dimers prefers PILOs in comparison to the stacking and C–H···π interactions.[13] Although these horizontal displaced orientations are weaker for 1 kcal/mol than stacking interactions, their frequent appearance can be explained by the effect of the crystal packing. High-level *ab initio* calculations on the benzene dimers demonstrate that mutual displacement of the benzene rings at large offsets allows a greater contact surface for additional interactions with the surrounding molecules, thus contributing to further stabilization of the supramolecular structure.[13] As an illustration of these effects, the crystal structure of the studied compound was reviewed with the emphasis on the cases where the molecules formed PILOs simultaneously with C–H···$\pi$ and C–H···O interactions. The C–H···$\pi$ interactions observed in motif VII (Table 1) is additionally stabilized by two C–H···O interactions and one PILO. The relative position of the molecules in motif III enabled the

aromatic rings to build, besides the PILO, both bifurcated C–H···O and C–H···$\pi$ interactions. In motif II, two 4-methoxybenzyl groups formed a PILO together with two C–H···O and two C–H···$\pi$ interactions. There were also two PILOs between two 4-methoxybenzyl groups and two tetralin groups, accompanied with bifurcated C–H···O interactions in motif VI. A greater number of C–H···O and C–H···$\pi$ interactions is the main reason why the interaction energy of motif III is higher than the interaction energy of motif VII. The preference for C–H···$\pi$ rather than for stacking interactions was rationalized in terms of larger contact surface of the interacting dimer. In the former case, there were three $\pi$-faces for interaction with the environment, while for stacked rings only two $\pi$-faces were accessible. Furthermore, the intermolecular interactions of tetralin and 4-methoxybenzyl units were compared in terms of their contribution to packing and stabilization of the crystal structure. All possible relative orientations of the tetralin, 4-methoxybenzyl and hydantoin units were extracted from motifs I–VII. The remaining parts were removed and H atoms were added in their place. The obtained models are presented in Figures 3 and 4 where ph and t in the labels indicate intermolecular interactions involving 4-methylanisole and tetralin, respectively. The Roman numerals in the labels of these new dimers referred to motifs I–VII from which they were derived. The numbers 1, 2 and 3 designate the individual relative orientations of 4-methylanisole and tetralin extracted from the same dimeric motif.

In the crystal packing, the 4-methoxybenzyl unit was surrounded by eight units (three tetralin, three 4-methoxybenzyl and two hydantoin rings) and formed 11 interactions (five C–H···$\pi$, four C–H···O interactions and two PILOs). The model systems shown in Figure 3 corresponds to these interactions. The results of calculations performed on these model systems show that C–H···$\pi$ interactions (ph.III-1, ph.V-1, ph.V-2, and ph.VII model systems) made the largest contribution in the stabilization of the crystal structure (total interaction energy –13.7 kcal/mol).

Further, C–H···O interactions (ph.III-2, ph.IV, and ph.V-3 model systems) with total interaction energy of –5.5 kcal/mol contributed more than PILOs (ph.III-1 and ph.VI model systems) with interaction energy of –4.0 kcal/mol. Total contribution to the stabilization equals –23.15 kcal/mol. Interestingly, only one of eleven interactions involved the π system of the 4-methoxybenzyl unit (ph.V-2 model system), while the methoxy O atom acted as an acceptor in weak C–H···O hydrogen bonding (ph.IV model system).

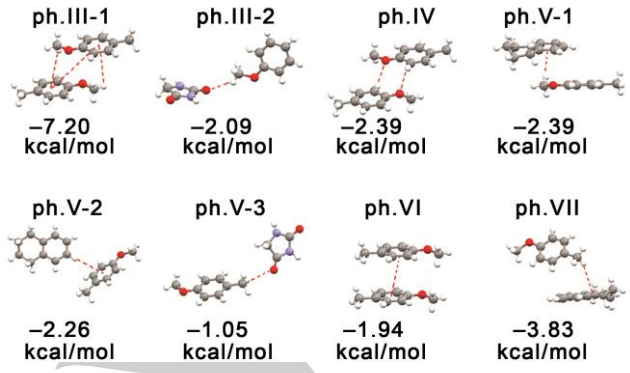


**Figure 3.** Model systems for evaluation of intermolecular interactions involving the 4-methoxybenzyl group observed in the crystal packing and interaction energies.

Namely, in these latter interactions the 4-methoxybenzyl unit mainly participated as a donor (eight interactions), whereby the methoxy H atoms were involved in three model systems (ph.III-1, ph.III-2, and ph.V-1 model systems), the benzylic methylene group in two model systems (ph.V-3 and ph.VII model systems) and the aromatic C–H in only one model system (ph.IV model system).

On the other hand, the tetralin unit was surrounded by nine units (four hydantoin, three 4-methoxybenzyl and two tetralin rings) through establishment of nine intramolecular interactions (four C–H···O, three C–H···π interactions and two PILOs). The model systems shown in Figure 4 represent intermolecular tetralin–tetralin and tetralin–hydantoin interactions. The results of the calculations performed on the model systems showed that C–H···π interactions (ph.V-1, ph.V-2, and ph.VII model systems) made the largest contribution to the stabilization of the crystal packing (total contribution of −8.5 kcal/mol). A slightly smaller contribution (about −8.1 kcal/mol) derived from C–H···O interactions (t.II-2, t.V-1, t.V-2, and t.VI-1 model systems). In this case, PILOs (t.II-1 and t.VI-2 model systems) had the smallest contribution to stabilization of the crystal packing (total contribution of −5.0 kcal/mol). The interactions involving tetralin had a total contribution to stabilization of −19.43 kcal/mol. In more detail, the π-system of the benzene unit was involved in only two interactions (ph.V-1 and ph.VII model systems), five interactions included tetralin ring system as a hydrogen-bonding donor, of which aliphatic C–H groups were involved in three model systems (t.II-2, t.V-1, and t.VI-1 model systems).

Finally, aromatic C–H groups participated in interactions of two model systems (ph.V-2 and t.V-2 model systems). PILO between an aromatic and aliphatic ring (t.VI-2 model system) were stronger than PILO between two aliphatic rings (t.II-1 model system).

The differences in the number of the contacts in the environment of the tetralin unit (nine units) and the 4-methoxybenzyl unit (eight units) can be attributed to the larger contact surface of tetralin (156.4 Å$^2$) relative to 4-methylanisole (149.1 Å$^2$). On the other side, this latter unit provided a slightly greater contribution to the overall stabilization of the crystal structure as a result of the nature of oxygen atom and methoxy group flexible orientation.

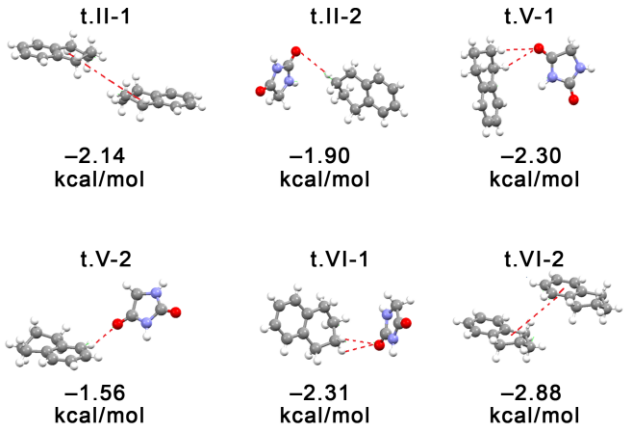


**Figure 4.** Model systems for evaluation of intermolecular tetralin–tetralin and tetralin–hydantoin interactions involving the tetralin unit observed in the crystal packing and the interaction energies.

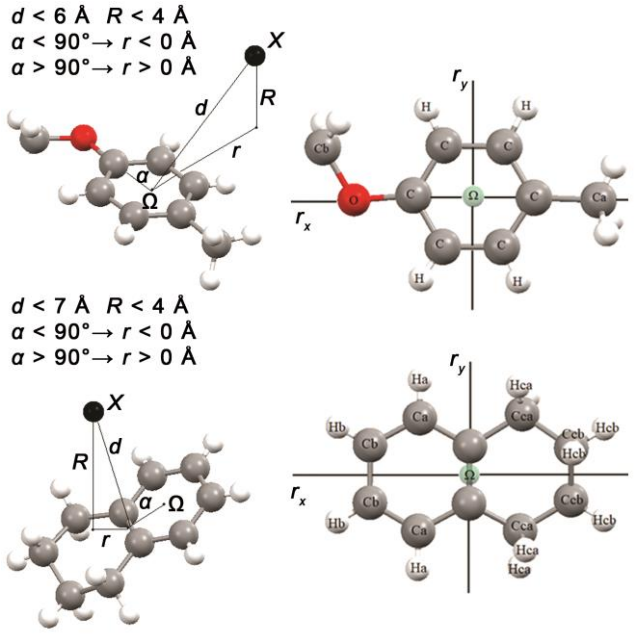


**Scheme 1.** Geometrical parameters used to define the contacts with the 4-methylanisole and tetralin fragments in the crystal structures from the CSD. The distance between an atom (X) and the centroid of the aromatic ring (Ω) is denoted as the parameter d, while R is the normal distance of an atom (X) to the plane of the aromatic ring. The parameter r is the distance between the centroid (Ω) of the 4-methylanisole ring and the projection of an atom (X) on the plane of the aromatic ring. In the case of the tetralin fragment, the distance d is defined from the centre of the carbon–carbon bond ($C_\Omega$) of the fused rings, while the parameter r is defined as the distances from the centre of the carbon–carbon bond ($C_\Omega$) to the projection of an atom (X) on the plane of the aromatic ring. For the 4-methylanisole ring, the parameter a is the angle formed by an atom X, the centroid of the aromatic ring (Ω) and the C19 atom, while, in the case of the tetralin ring system, it is the angle formed by atom X, the centre of the carbon–carbon bond (CΩ) and the centroid of the aromatic ring (Ω). In the C6-aromatic ring, the distance from the ring centroid (Ω) to the centre of the carbon–carbon bond (CΩ) and the carbon atom are about 1.2 and 1.4 Å, respectively.

**Statistical analysis of the crystal structures from the Cambridge Structural Database.** To confirm whether our conclusions derived from the analysis of intermolecular interactions in the crystal structure of the studied compounds follow a general trend, we additionally performed a statistical analysis of the data relating to the 4-methylanisole and tetralin ring systems extracted from the CSD.

Based on the geometrical criteria defining the contact space in Scheme 1, the CSD survey revealed 3903 atoms in this space involving the fragment that corresponded to 4-methylanisole (a H atom was removed from the methoxy group). In the described contact space ($d$ < 6 Å and $R$ < 4 Å), the most abundant were the H atoms (1803 contacts), C($sp^2$) atoms (1299 contacts), C($sp^3$) atoms (387 contacts) and O atoms (253 contacts). A statistical distribution was performed for every atom according to the offset value ($r$ parameter, Figure 5). To facilitate the identification of the interaction type, the $r$ parameter was decomposed into two components $r_x$ and $r_y$ according to $r^2=r_x^2+r_y^2$ (Figure S1). The parameter $r_x$ is the component of the $r$ parameter, which represented the projection onto the axis passing through the centroid of the aromatic ring (Ω) and the C atoms bearing the methoxy and methyl substituent. The component $r_y$ was its projection onto the axis perpendicular to the former one and was located in the plane of the aromatic ring (Figure S1). The H and C atoms were located at offsets larger than 2.0 Å that refers to their tendency to position outside of aromatic ring. Namely, all four atoms have the maxima of distributions at offsets with absolute values greater than 4 Å which, corresponded to hydrophobic interactions in the case of the H atoms, C($sp^2$) atoms and C($sp^3$) atoms. As the methoxy O atoms were located at offsets close to 2.8 Å, a part of these contacts (with the negative r parameter values) were C–H···O interactions. Concerning the distribution of the r parameter for the O atom, there was a tendency towards offsets with absolute values greater than 3 Å as a consequence of C–H···O interactions. However, when the values of the $r_x$ component were taken into account, it was obvious that the majority of these interactions involved the C–H groups of the aromatic ring ($r_x$ in the range from –2 to 2 Å) and then from the methyl group ($r_x$ greater than 2 Å). C–H···O interactions which involved the methoxy C–H groups ($r_x$ less than –2 Å) were the smallest in number. The greatest tendency to position above the aromatic ring had the H and C($sp^2$) atoms, thus reflecting X–H···$\pi$ and $\pi$–$\pi$ interactions. Nevertheless, the C($sp^2$) atoms tended toward the r values greater than 4 Å which can be ascribed to PILOs and hydrophobic interactions (recognized by the values of the $r_y$ parameter greater than 4 Å). The peak for the $r$ parameter at about 4 Å originated from C–H···π interactions of the methyl group (for the $r_x$ values greater than 2.5 Å), while the lower peak at about –4 Å came from the C–H···$\pi$ interactions of the methoxy group (for the $r_x$ values less than –3 Å). C–H···O interactions involving the methoxy group were smaller in number than interactions with the methyl group (the $r_x$ values less than –2 Å).

Within the tetralin ring system, the coordinate origin was placed at the center of mass between two C atoms belonging to both benzene and non-aromatic six-membered rings (the center of the carbon–carbon bond ($C_\Omega$) of the fused rings). An axis passing through these atoms was taken for the $y$-axis, while a perpendicular axis in the plane of the benzene ring was considered as the $x$-axis (Figure S2). Within the contact space of the tetralin ring system ($d$ < 7 Å and $R$ < 4 Å, Scheme 1), 682 contacts were found, whereby the H atoms (300 contacts), the C($sp^3$) atom (179 contacts), the C($sp^2$) atom (49 contacts) and the O atoms (17 contacts) were the largest in number. Interestingly, the contacts involving the non-aromatic six-membered ring of the tetralin system ($r$ > 0) were larger in number than those involving the benzene ring ($r$ < 0). In the case of the tetralin ring system, intermolecular interactions with atoms above the ring (the $r_x$ values in the range from –3 to 3 Å and $r_y$ values in the range from –2 to 2 Å, Figure S2) were less abundant than for the 4-methylanisole ring. Hydrophobic interactions were the most common among contacts involving the H, C($sp^3$) and C($sp^2$) atoms ($r$ < –5 Å and $r$ > 5 Å). When the contribution of the contacts involving the O atom was taken into account (6.5 and 2.5% for anisole and tetralin, respectively), it can be concluded that the tetralin ring system had a lower affinity towards the O atom, i.e., C–H···O interactions. In comparison to the anisole ring, the tetralin ring system had also a lower affinity towards the C($sp^2$) atom, i.e., $\pi$-interactions.

**Drug-likeness.** The concept of drug-likeness offers a useful guideline in accessing the pharmacokinetic profile of a pharmacologically active compound in the early stages of the drug discovery.[14] The rule of five uses cheminformatic

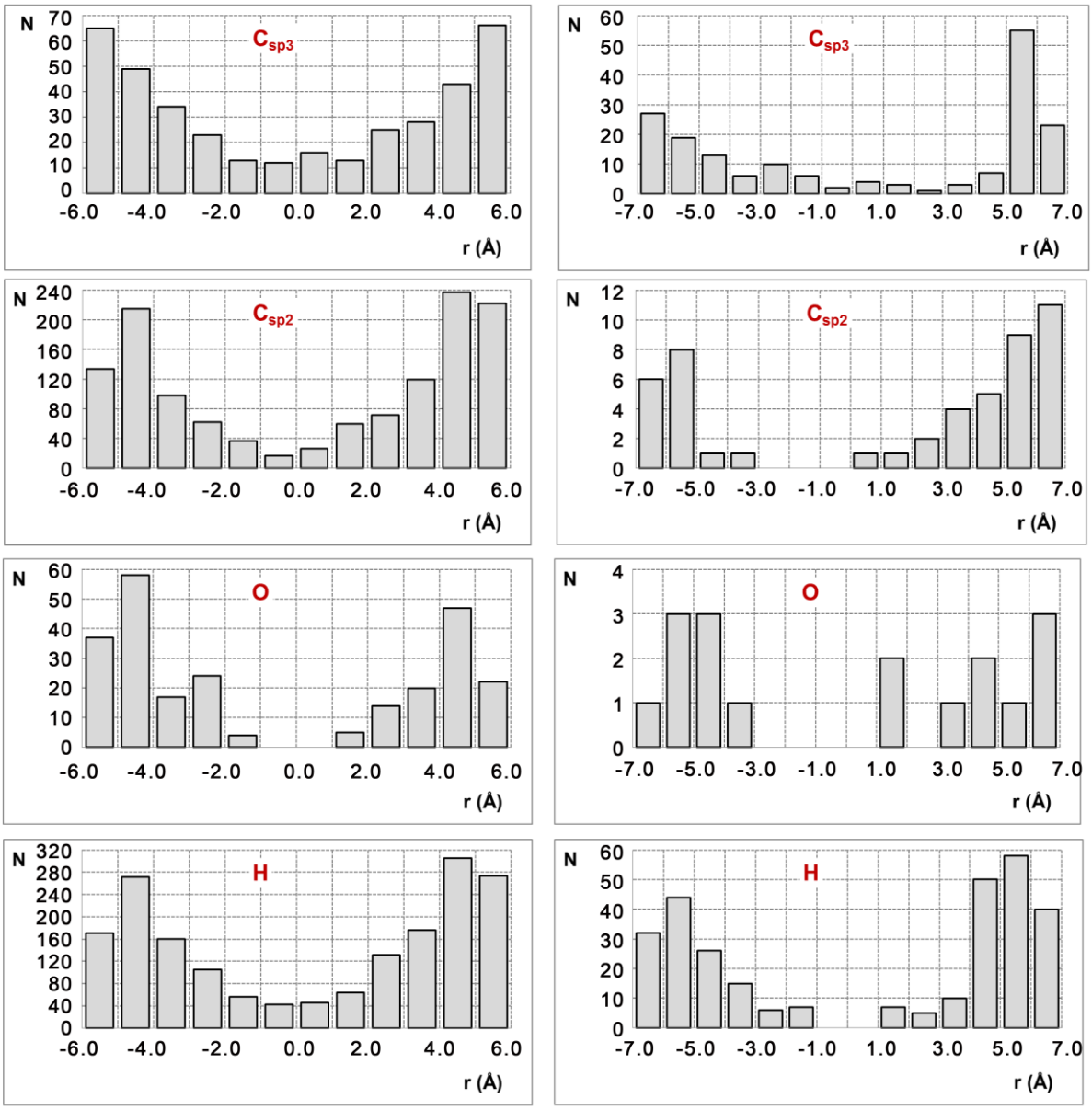


**Figure 5.** Distribution of the *r* parameter for the C($sp^3$), C($sp^2$), O and H atoms within the contact space around 4-methylanisole (left column) and the tetralin ring system (right column).

drug-likeness filters, such as molecular weight (*MW*) ≤ 500, log*P* ≤ 5, number of hydrogen bond donors ($N_{HB}$(D)) ≤ 5, number of hydrogen bond acceptors ($N_{HB}$(A)) ≤ 10. According to this rule, a molecule will not be orally active if it violates two or more rules.[15]

Drug-likeness of the studied compound was evaluated through the Rule of five and its extensions that define a boundaries for pharmacologically active compound, *i.e.*, the Ghose criterion (160 ≤ *MW* ≤ 480; −0.4 ≤ Wlog*P* ≤ 5.6; 40 ≤ molar refraction (*R*m) ≤ 130; 20 ≤ number of atoms ($N_A$) ≤ 70), Egan's criterion (Wlog*P* ≤ 5.88; topological polar surface area (TPSA) ≤ 131.6 Å$^2$)[16] and Veber's criterion (number of rotatable bonds ($N_{RB}$) ≤ 10; TPSA ≤ 140 Å$^2$ and total $N_{HB}$(D) and $N_{HB}$(A)≤ 12))[17] using Molinspiration,[18] Swissadme,[19] and Swissdock.[20] The studied compound passed all these *in silico* models (Table 2) and had properties that would make it likely orally active. Its moderate lipophilicity (Wlog*P* = 1.96, calculated according to reference[20]) and a low value of the polar surface area (58.6 Å$^2$) underlined increased permeation through the biological membranes. The low number of hydrogen bond donors and acceptors indicated that this compound exhibited relatively low capacity for hydrogen bonding toward proton donating and accepting groups of the target. Furthermore, three rotatable bonds suggested that larger conformational changes should not be expected upon its binding to the target.

According to data collected from the Swissdock program, the investigated compound can be characterized as potential inhibitor of Kinase enzymes and antigen (AG) protein-coupled receptors (Table S2, and Figure S3). Guided by this information, we performed a docking study on the Dopamine D3 receptor

**Table 2.** Physico-chemical properties of the studied compound.

| *MW* | $N_{RB}$ | $N_{HB}$(D) | $N_{HB}$(A) | $R_m$ | TPSA | log *P* (WLOG*P*) |
|---|---|---|---|---|---|---|
| 336.38 | 3 | 1 | 3 | 101.36 | 58.64 | 1.96 |

(pdb code: 3PBL),[21] and IRAK 4 (Interleukin-1 Receptor-Associated Kinase 4) enzyme (pdb code: 5UIU).[22]

The D3 receptor, a member of the D2-like receptor family, has attracted attention as pharmacological target, because dysfunction of the dopaminergic system is related to different neurological disorders.[23] Biochemical studies reveal that D3 receptors are negatively coupled to adenylyl cyclase and negatively modulate the activity of the protein kinase and its effectors.[23]

IRAK-4 is an integral part of the Interleukin-1-Receptor signaling cascade, the overactivation of which is linked with various autoimmune diseases, such as cancer, psoriasis, rheumatoid arthritis and systemic lupus erythematosus.[24] Hence, the inhibitors of IRAK4 might have the anti-inflammatory activity and the activity associated with weakening the innate immune response.

**Results of docking study.** Elucidating the pharmacological properties of a chemical compound by molecular docking has nowadays been a growing and helpful research practice. The results of the docking study for (*S*)-enantiomer showed that the investigated compound had three binding sites at the Dopamine D3 receptor (Figure 6a). Two binding sites for (*S*)-enantiomer were in the *trans*-membrane region, the first one was on the extracellular side (binding energy of −8.7 kcal/mol) and the other one was on the intracellular side (binding energy of −7.9 kcal/mol). The third binding site was located in the intracellular domain (binding energy of −8.3 kcal/mol). In addition to the highest binding energy (−8.7 kcal/mol) and the highest conformational freedom (7 conformers), the binding site of the test compound was in the antagonist binding cavity, deep in the seven trans-membrane bundle. The (*S*)-enantiomer of the tested compound bound to the D3 receptor at the junction of helices I, II, and VII, which is known as the second extracellular binding pocket.[24] According to the docking results, the investigated compound blocked the D3 receptor, thus preventing inhibition of adenyl cyclase. The tested compound had a slightly higher affinity for the IRAK4 enzyme (Interleukin-1 Receptor-Associated Kinase 4), with a binding energy of −9.4 kcal/mol (Figure 6b). In addition, the compound showed high selectivity for binding to the active site of the enzyme. The binding of this compound inhibited the action of the enzyme, that is, reduces its activity. The docking results for the (*R*)-enantiomer were consistent with the docking results for the (*S*)-enantiomer in terms of the number and position of binding sites on the tested enzymes (Figure 6). There was a slight difference in the binding energies. Namely, the (*R*)-enantiomer has slightly higher binding energies for Dopamine D3 receptor (energies of −9.2, −8.3, and −8.2 kcal/mol), and slightly smaller binding energy for the IRAK4 (−9.2 kcal/mol) in comparison to the (*S*)-enantiomer. Despite slight differences, similar activities of the (*R*)- and (*S*)-enantiomers are expected.

**Affinity of the tetralin ring system and 4-methoxybenzyl group towards amino acids and interactions.** Using the "Find residues close to selection" option in Discovery Studio, we analyzed the AA environment of the tetralin and 4-methoxybenzyl units at the binding sites of the studied enzymes (Table 3 and 4). The total analysis of the AA residues, shown as a function of their nature (polar, nonpolar, positive and negative) and the type of interactions which these groups establish with the AA residues, is also studied. A more detailed description is given in Supporting Information (Table S3, S4 and S5, Figure S4 and S5).

In addition to hydrophobic interactions, which were the most abundant, in the first binding site (BS1) at IRAK4 enzyme (Table 3), the tetralin ring system established three C–H···O interactions (with *Ser269*, *Glu194* and *Asp272*), as a donor of the C–H bond, and two interactions including the *π*-system of the ring (N–H···*π* interaction with *Glu194* and C–H···π interaction with *Ala315*). The 4-methoxybenzyl group mostly formed hydrophobic interactions; however, due to the low strength of these interactions, their contribution in the total binding energy was insignificant. This ring formed three C–H···O interactions, two interactions wherein the methoxy O atom was a hydrogen bonding acceptor (interactions with *Leu318* and *Ala211*) and one wherein the methoxy C–H group was a hydrogen bonding donor (interaction with *Met265*). The group also formed two C–H···*π* interactions, one as a C–H donor (interaction with *Tyr262*) and the second as a π-acceptor of hydrogen bonding (interaction with *Val200*). The 4-methoxybenzyl group interacted mainly with non-polar AAs, while the tetralin ring system had a slightly higher affinity to polar and charged AAs.

The number of interactions in the first binding site (BS1) with AA residues from the D3 receptor was significantly smaller (Table 4). In this case, the studied compound was bound in the channel

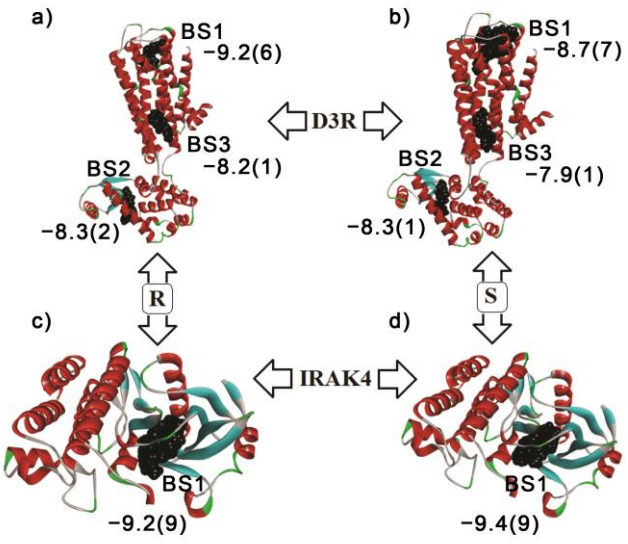


**Figure 6.** The binding sites, the corresponding binding energies, and the number of conformers for the specific binding sites of the test compound with the *R* configuration (a and c) and the *S* configuration (b and d) at the D3 dopamine receptor (a and b) and the Interleukin-1 Receptor-Associated Kinase 4 (IRAK4, c and d).

**Table 3.** Interactions of the tetralin and 4-methoxybenzyl groups with amino acids at the binding sites obtained by docking study at IRAK4.

| Configuration | Binding site (BS) | Tetralin ring system | | 4-Methoxybenzyl group | |
|---|---|---|---|---|---|
| | | Amino acid | Interactions | Amino acid | Interactions |
| *R* | BS1 | *Leu271* | HP | *Leu318* | HP; C–H···O |
| | | *Gly195* | HP | *Met265* | HP; C–H···O |
| | | *Ala315* | C–H··· *π* | *Val200* | C–H···*π* |
| | | *Ser269* | HP; C–H···O | *Ala211* | HP; C–H···O |
| | | *Glu194* | C–H···O; N–H···*π* | *Met192* | HP |
| | | *Asp272* | C–H···O | *Tyr262* | C–H···*π* |
| | | *Lys313* | HP | *Lys213* | HP |
| *S* | BS1 | *Phe197* | HP; PILO | *Ala315* | C–H···O |
| | | *Gly196* | HP | *Val200* | C–H···*π* |
| | | *Gly195* | C–H···*π* | *Gly193* | HP |
| | | *Gly198* | C–H···O; C–H···N | *Met192* | HP |
| | | *Ala315* | HP | *Leu318* | C–H···*π* |
| | | *Asn316* | C–H···O | *Ala211* | C–H···O |
| | | *Asp329* | C–H···O | *Gly268* | HP |
| | | *Lys313* | HP | *Met265* | HP; C–H···O |
| | | *Lys213* | HP | *Ser269* | HP |
| | | | | *Tyr264* | HP |

* HP = Hydrophobic interactions.

close to the enzyme surface, whereas in the case of IRAK4 enzyme, the binding site was located much deeper within the enzyme. Both units mostly formed hydrophobic interactions, although there was a significant difference in the interaction profile of these two rings.

Namely, the tetralin ring system established additional two interactions involving its *π*-system (C–H···*π* interaction with *Phe345* and anion···*π* interaction with *Asp110*). On the other hand, the 4-methoxybenzyl group had a slightly higher affinity for C–H···O interactions (interactions with *Cys181* and *Glu90*), wherein the 4-methoxybenzyl group has a role of C–H donor. In addition, this group formed C–H···*π* interaction with *Leu89*. When analyzing the nature of interactions with AAs from the D3 receptor, one can conclude that there is a slight difference in

**Table 4.** Interactions of the tetralin and 4-methoxybenzyl groups with amino acids at the binding sites obtained by docking study at the D3 receptor.

| Configuration | Binding site (BS) | Tetralin ring | | 4-methoxybenzyl group | |
|---|---|---|---|---|---|
| | | Amino acid | Interactions | Amino acid | Interactions |
| *R* | BS1 | *Ile183* | HP | *Leu89* | C–H···*π* |
| | | *Trp373* | HP | *Phe106* | HP |
| | | *Phe345* | C–H···*π* | *Val86* | HP |
| | | *Thr369* | HP | *Ser182* | HP |
| | | *Asp110* | Anion···*π* | *Cys181 Glu90* | HP; C–H···O |
| | | | | | C–H···O |
| | BS2 | *Ala1073* | HP | *Gly1030* | C–H···O |
| | | *Phe1104* | C–H···*π* C–H···O | *Leu1032* | HP; N–H···*π* |
| | | *Val1103* | HP; C–H···O | *Gln1105* | HP; C–H···O |
| | | *Asp1070* | HP; C–H···O | *Tyr1018* | C–H···O |
| | | | | *Thr1026* | HP |
| | | | | *Glu1011* | C–H···O |
| | | | | *Asp1020* | HP; C–H···O |
| | BS3 | *Val205* | HP; C–H···O | *Leu215* | HP |
| | | *Leu335* | HP | *Thr328* | HP; C–H···O |
| | | *Ala332* | HP | *Gln329 Lys325* | HP; HB |
| | | *Ala209* | HP; C–H···N | | HP; C–H···O |
| | | *Tyr208* | C–H···*π* Stacking | | |
| *S* | BS1 | *Pro362* | HP | *Val86* | C–H···*π* |
| | | *Ser366* | O–H···*π* | *Leu89* | HP |
| | | *Tyr365* | HP | *Phe106* | HP; C–H···O |
| | | *Glu90* | C–H···O | *Thr369* | HP |
| | | | | *Tyr373 Asp110* | HP; C–H···O |
| | | | | | C–H···O |
| | BS2 | *Ala1074* | HP | *Gly1030* | C–H···*π* |
| | | *Phe1104* | Stacking | *Leu1032* | HP |
| | | *Val1103* | HP; C–H···O | *Thr1026* | C–H···O |
| | | *Gly1030* | C–H···O | *Gln1105* | HP F |
| | | *Leu1032* | HP; C–H···N | *Tyr1018* | HP; HB |
| | | *Asp1070* | HP; C–H···O | *Glu1011* | C–H···O |
| | | *His1031* | HP | *Asp1020* | HP; C–H···O |
| | BS3 | *Ala332* | HP | *Ala332* | C–H···O |
| | | *Ile211* | C–H···*π* | *Leu335* | HP; C–H···O |
| | | *Leu215* | C–H···*π* | *Ile339* | HP |
| | | *Gln329* | HP; C–H···N | *Tyr212* | HP; C–H···O |
| | | *Thr328* | HP; C–H···O | *Tyr208* | Stacking |
| | | *Tyr212* | HP; C–H···*π* | | |
| | | *Tyr208* | HP | | |
| | | *Arg218* | HP | | |

* HP= Hydrophobic interactions, HB= Hydrogen bond.

preference of analyzed rings for a particular type of interactions. To achieve a more comprehensive insight, the interactions with AAs were analyzed for all binding sites. An analysis of the nature of the AA residues around the tetralin ring system revealed that interactions with nonpolar groups were the most prevalent and even more numerous than interactions with other AA residues (polar, positive and negative). The second-largest group of interaction involved the polar AA residues. Interactions with positive AA residues were the least represented. When considering the types of interactions, hydrophobic interactions (32 interactions) were the most prevalent. C–H···O, C–H···$\pi$ and C–H···N interactions were significantly less represented (15, 7, and 4 interactions, respectively). In addition to these, $\pi$···$\pi$ stacking, O–H···$\pi$, N–H···$\pi$, PILO, anion···$\pi$ interactions occurred, but with a very little frequency (1 or 2 interactions only). The total number of interactions is 64, only 12 of which interacted with the π-system of the tetralin ring system (interacting atoms above the ring). This distribution correlated well with the data obtained from the CSD analysis for the tetralin ring system, which indicated a high number of hydrophobic interactions and a small contribution of interactions with atoms above the tetralin ring system.

Similar to the tetralin unit, the 4-methoxybenzyl group was mostly surrounded by the non-polar AA residues. Also, these AA residues were more numerous than the sum of the others. The second most represented ones were polar, while the least represented were positive AA residues. Unlike for the tetralin ring system, the number of polar AAs in the environment of the 4-methoxybenzyl group increased, while the number of positive AAs decreased. The total number of AAs, which interact with the 4-methoxybenzyl group (52 AAs), was slightly larger than the number of AAs in the neighborhood of the tetralin ring system (49 AAs), although the surface area of the 4-methoxybenzyl group is smaller. The explanation can be based on the greater flexibility of the 4-methoxybenzyl group (greater number of rotatable bonds) which made it more adaptable for interactions with biological targets. Also, hydrophobic interactions are the most numerous (35 interactions), while C–H···O, C–H···$\pi$ interactions and hydrogen bonds are significantly less represented (25, 7, and 2 interactions, respectively). Besides that, the 4-methoxybenzyl group formed one $\pi$···$\pi$ stacking, and one N–H···$\pi$ interaction. In comparison to the tetralin ring system, the number of C–H···O interactions increased, although the number of the C–H groups within these units was similar. The reason for this is the participation of the methoxy O atom which acts as an acceptor in C–H···O interactions. Similar to the number of AA residues, the number of interactions formed by the 4-methoxybenzyl group (71 interactions) was slightly larger than the number of interactions with the tetralin ring system (64 interactions).

Such a distribution was derived from the greater flexibility of the 4-methoxybenzyl group. The contribution of interactions involving the $\pi$-system (9 of 71 interactions) was lower than in the case of the tetralin ring system. A qualitative correlation between the docking study results and the results of the CSD analysis can be drawn and showed a high affinity of the 4-methoxybenzyl group towards hydrophobic interactions and a low abundance of interactions with atoms or species above the aromatic ring.

## Conclusion

In this work, the hierarchical development of the crystal structure of a racemic spirohydantoin derivative was discussed through cooperativity of various homo and heterohiral dimeric motifs associated with the presence of different intermolecular interactions, namely strong N–H···O, and weaker C–H···O, C–H···$\pi$ and PILOs. These motifs link molecules into alternating double layers, wherein the planes of the hydantoin rings of the adjacent double layers are mutually perpendicular. When comparing contributions of the tetralin and 4-methoxybenzyl units in the formation of the crystal structure, it seems that a larger number of the contact fragments in the environment of the tetralin unit results from its larger contact surface. On the other side, the 4-methoxybenzyl unit provides a slightly greater contribution to the total interaction energy, i.e., to the overall stabilization of the crystal packing. Thus, a statistical analysis of the data relating to the 4-methylanisole and tetralin ring systems extracted from the CSD revealed that the H, C, and O atoms were the largest in number within the contact area. These atoms were mainly located outside the ring, indicating that these atoms did not have tendency to interact with position above the ring. For the 4-methoxybenzyl unit, these atoms had a tendency towards offsets greater than 4 Å, as a consequence of hydrophobic interactions (in the case of the H atoms and C($sp^3$) atoms), PILOs and C–H···$\pi$ interactions (in the case of C($sp^2$) atoms) as well as C–H···O interactions (in the case of the O atoms). Within the tetralin ring system, interactions involving the non-aromatic six-membered ring ring were more numerous than the interactions with the benzene ring. Interactions with atoms above the ring are less abundant than in the case of the 4-methylanisole ring. Hydrophobic interactions were also the most common among contacts involving the H, C($sp^3$) and C($sp^2$) atoms. In comparison to the 4-methylanisole unit, the tetralin ring system had also a lower affinity towards the O atom (for C–H···O interactions) and C($sp^2$) atom (for interactions involving the $\pi$-system and PILOs).

Regarding the pharmacological potential of the investigated compound, it was recognized as a potential inhibitor of Kinase enzymes and AG protein-coupled receptors. The total number of AAs, which interact with the 4-methoxybenzyl unit, was slightly larger than the number of AAs in the neighborhood of the tetralin unit as a result of its greater flexibility. It made the 4-methoxybenzyl unit more adaptable for interactions with the biological targets. Furthermore, the investigated compound fulfilled the criteria of Lipinski and its extensions and is more likely to have the characteristics that are important for a potent, bioavailable drug. Encouraged by the obtained results, we are currently working to introduce substituents other than the methoxy group into the benzylic unit to investigate the self-assembly behavior and pharmacological potential of a series of spirohydantoins derived from α-tetralone.

## Experimental Section

**Synthesis of 3-(4-methoxybenzyl)-6,7-benzo-1,3-diazaspiro[4.5]decane-2,4-dione.** Unless otherwise noted, all starting materials, reagents and solvents were obtained from commercial suppliers and used without further purifications. The synthetic route was carried out according to Scheme 2. Strting from commercially

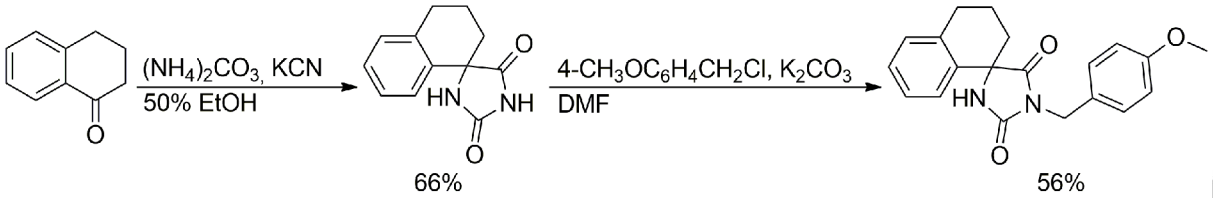


**Scheme 2.** Synthesis of 3-(4-methoxybenzyl)-6,7-benzo-1,3-diazaspiro[4.5]decane-2,4-dione.

available α-tetralone, the modified Bucherer-Bergs reaction was achieved by the use of ammonium carbonate and potassium cyanide to afford the 3',4'-dihydro-2H-spiro[imidazolidine-4,1'-naphtalene]-2,5-dione.[25] In the following step, alkylation at position 3 of the hydantoin ring was carried out with 4-methoxybenzyl chloride in presence of $K_2CO_3$ in *N*,*N*-dimethylformamide.[26]

**Table 5.** Crystal and structure refinement data for 3-(4-methoxybenzyl)-6,7-benzo-1,3-diazaspiro[4.5]decane-2,4-dione.

| | |
|---|---|
| Formula | $C_{20}H_{20}N_2O_3$ |
| Formula weight, g mol$^{-1}$ | 336.38 |
| Crystal size, mm$^3$ | 0.90 × 0.46 × 0.11 |
| Crystal system | Monoclinic |
| Space group | $P2_1/c$ |
| *a*, Å | 12.682(3) |
| *b*, Å | 6.4556(13) |
| *c*, Å | 20.839(4) |
| *β*, ° | 98.62(3) |
| *V*, Å$^3$ | 1686.8(6) |
| *Z* | 4 |
| *F*(000) | 712 |
| *μ*, mm$^{-1}$ | 0.09 |
| $\rho_c$, g cm$^{-3}$ | 1.325 |
| $\theta$ range, ° | 2.741–25.348 |
| Index ranges, *h*, *k*, *l* | –15→14<br>–7→7<br>–22→25 |
| Reflections collected/unique | 6567/3083 |
| Data/restraints/parameters | 2379/0/226 |
| *R* indices [$I > 2\sigma(I)$] | $R = 0.0409$, $R_w = 0.094$[a] |
| *R* indices (all data) | $R = 0.0582$, $R_w = 0.1034$ |
| Goodness-of-fit | 1.048 |
| $R_{int}$ | 0.0183 |
| $\Delta\rho_{max}$, $\Delta\rho_{min}$, e Å$^{-3}$ | 0.125, –0.158 |

[a] $w = 1 / [\sigma^2(F_o^2) + (0.0445 \cdot P)^2 + 0.3159 \cdot P]$ where $P = (F_o^2 + 2 \cdot F_c^2) / 3$.

The obtained compound were completely structurally characterized by the determination of melting point, FT-IR, $^1$H and $^{13}$C NMR and elemental analysis. The melting point was measured on an Electrothermal melting point apparatus without correction. The FT-IR spectrum of the synthesized compounds was recorded in the range of 400 to 4000 cm$^{-1}$ using Bomem MB spectrophotometer. The $^1$H NMR spectrum was measured with a Bruker AC 250 spectrometer on 400 MHz, while $^{13}$C NMR spectrum was recorded at 100 MHz on the same device. All spectra were recorded at room temperature in DMSO-$d_6$. Elemental analysis of the investigated compound was carried out using microanalyzer Elemental Vario EL III.

**X-ray structure determination.** Single-crystal X-ray diffraction data of 3-(4-methoxybenzyl)-6,7-benzo-1,3-diazaspiro[4.5]decane-2,4-dione were collected at 293 K on an Oxford Gemini S diffractometer equipped with a CCD detector using monochromatized MoKα radiation (λ = 0.71073 Å). Intensities were corrected for absorption using the multi-scan method. Because of the dimensions of the single crystal (Table 4), additional Gaussian correction for absorption was applied. The structure was solved by direct methods (SHELXT-2018/2),[27] and refined on F2 by full-matrix least-squares using the programs SHELXL-2018/3,[28] and WINGX.[29] All non-hydrogen atoms were refined anisotropically. Positions of the H atoms connected to the C and N atoms were calculated on geometric criteria and refined using the riding model with Uiso = 1.2Ueq(C, N) and Uiso = 1.5Ueq(C) for the methyl group. Selected crystal data and refinement results for 3-(4-methoxybenzyl)-6,7-benzo-1,3-diazaspiro[4.5]decane-2,4-dione are listed in Table 5. Crystallographic data reported in this paper have been deposited with the Cambridge Crystallographic Data Centre as supplementary publication No. CCDC 1986009. Copy of the data can be obtained, free of charge, *via* https://www.ccdc.cam.ac.uk/structures/.

**Computational details** All quantum-chemical calculations were performed using TPSS functional with Grimme's D3 dispersion correction method and def2tzvp basis set, as implemented in the Gaussian09 program package.[30] Basis set superposition error (BSSE) was corrected for calculated interaction energies based on Counterpoise method.[31] The statistical analysis of intermolecular interactions was based on structures extracted from the CSD version 5.36.[12] The program *ConQuest* 1.10[32] was used to retrieve structures from the CSD, which satisfied the geometrical criteria shown in Scheme 1, as well as the following criteria: (*i*) error-free coordinates according to the criteria used in the CSD; (*ii*) not disordered structures; (*iii*) the H atom positions were normalized using the CSD default bond lengths; (*iv*) no powder structures; (*v*) no polymer structures; (*vi*) determined 3D coordinates, (*vii*) the crystallographic *R* factor is lower than 10%. The website of Swiss Institute of Bioinformatics[33] was used to compute physico-chemical descriptors and to predict ADME parameters. This website was also used to predict the most probable biomolecular targets of the investigated compound, assumed as a bioactive ligand. Docking study of flexible ligands, (*S*)-3-(4-methoxybenzyl)-6,7-benzo-1,3-diazaspiro[4.5]decan-2,4-dione and (*R*)-3-(4-methoxybenzyl)-6,7-benzo-1,3-diazaspiro[4.5]decan-2,4-dione), and rigid targets were performed using the *AutoDockTools* program and *AutoDock Vina* suite of programs.[33] The structures of biomolecules were obtained from the Protein Data Bank.[34] The analysis of amino acid environment of the flexible ligands at the binding sites of the enzymes was archived by *Discovery Studio* simulation tools.[35]

## Acknowledgements

This work was supported by the Ministry of Education, Science and Technological Development of the Republic of Serbia (Contract No. 451-03-68/2020-14/200135, 451-03-68/2020-14/ 200287 and 451-03-68/2020-14/200026).

**Keywords:** Chiral recognition • Drugs • Fragment-based analysis • Molecular docking • Noncovalent interactions

[1] A. Gavezzotti, S. Rizzato, *J. Org. Chem.* **2014**, *79*, 4809–481.
[2] W. Peng, F. Ding, *Mol. Biosyst*. **2017**, *13*, 2226–223.
[3] P.R. Spackman, L. Yu, C. J. Morton, M. W. Parker, C. S. Bond, M. A. Spackman, D. Jayatilaka, S. P. Thomas, *Angew. Chem. Int. Ed.* **2019**, *58*, 16780–16784.
[4] S. H. Cho, S. H. Kim, D. Shin, *Eur. J. Med. Chem*. **2019**, *164*, 517–545.
[5] T. Mendgen, C. Steuer, C. D. Klein, *J. Med. Chem*. **2012**, *55*, 743–753.
[6] G. M. Lipkind, H. A. Fozzard, *Mol. Pharmacol*. **2010**, *78*, 631–638.
[7] K. Kucwaj-Brysz, R. Kurczab, M. Jastrzębska-Więsek, E. Żesławska, G. Satała, W. Nitek, A. Partyka, A. Siwek, A. Jankowska, A. Wesołowska, K. Kieć-Kononowicz, J. Handzlik, *Eur. J. Med. Chem*. **2018**, *147*, 102–114.
[8] W. Yu, Z. Guo, P. Orth, V. Madison, L. Chen, C. Dai, R. J. Feltz, V. M. Girijavallabhan, S. H. Kim, J.A. Kozlowski, B. J. Lavey, D. Li, D. Lundell, X. Niu, J. J. Piwinski, J. Popovici-Muller, R. Rizvi, K. E. Rosner, B. B. Shankar, N. Y. Shih, M. Arshad Siddiqui, J. Sun, L. Tong, S. Umland, M. K. C. Wong, D. Yang, G. Zhou, *Bioorg. Med. Chem. Lett.* **2010**, *20*, 1877–1880.
[9] L. Sacconnay, L. Ryckewaert, G. M. Randazzo, C. Petit, C. D. S. Passos, J. Jachno, V. Michailoviene, A. Zubriene, D. Matulis, P. A. Carrupt, C. A. Simões-Pires, A. Nurisso, *Eur. J. Pharm. Sci*. **2016**, *85*, 59–67.
[10] a) P. T. Todorov, R. N. Petrova, E. D. Naydenova, B. L. Shivachev, *Cent. Eur. J. Chem*. **2009**, *7*, 14–19; b) S. Graus, D. Casabona, S. Uriel, C. Cativiela, J. L. Serrano, *CrystEngComm* **2010**, *12*, 3132–3137; c) A. Lazić, N. Trišović, L. Radovanović, J. Rogan, D. Poleti, Ž. Vitnik, V. Vitnik, G. Ušćumlić, *CrystEngComm* **2017**, *19*, 469–483; d) A. M. Lazić, L. D. Radovanović, B. Đ. Božić, B. Đ. Božić Nedeljković, V. D. Vitnik, Ž. J. Vitnik, J. R. Rogan, N. V. Valentić, G. S. Ušćumlić, N. P. Trišović, *J. Mol. Struct*. **2019**, *1180*, 48–62.
[11] D. H. Setiadi, G. A. Chass, L. L. Torday, A. Varro, J. G. Papp, *J. Mol. Struct. Theochem.* **2002,** *594*, 161–172.
[12] C. R. Groom, I. J. Bruno, M. P. Lightfoot, S. C. Ward, *Acta Crystallogr. Sect. B: Struct. Sci. Cryst. Eng. Mater*. **2016**, *72,* 171-179.
[13] D. B. Ninković, G. V. Janjić, D. Ž. Veljković, D.N. Sredojević, S. D. Zarić, *Chemphyschem* **2011**, *12*, 3511–3514.
[14] L. Guan, H. Yang, Y. Cai, L. Sun, P. Di, W. Li, G. Liu, Y. Tang, *Medchemcomm* **2019**, *10*, 148–157.
[15] S. Mignani, J. Rodrigues, H. Tomas, R. Jalal, P. P. Singh, J. P. Majoral, R. A. Vishwakarma, *Drug Discov. Today* **2018**, *23*, 605–615.
[16] W. Egan, K. Merz, J. Baldwin, *J. Med. Chem.* **2000**, 43, 3867–3877
[17] N. S. El-Din, *World J. Pharm. Pharm. Sci*. **2017**, *6*, 1145–1160.
[18] https://www.molinspiration.com, (accessed November 2019).
[19] a) A. Daina, O. Michielin, V. Zoete, *Sci. Rep.* **2017**, *7*, No-42717; b) http://www.swissadme.ch, (accessed November 2019).
[20] http://www.swissdock.ch, (accessed November 2019).
[21] E. Y. T. Chien, W. Liu, Q. Zhao, V. Katrich, G. W. Han, M. A. Hanson, L. Shi, A. H. Newman, J. A. Javitch, V. Cherezov, R. C. Stevens, *Science* **2010**, *330*, 1091–1095.
[22] K. L. Lee, C. M. Ambler, D. R. Anderson, B. P. Boscoe, A. G. Bree, J. I. Brodfuehrer, J. S. Chang, C. Choi, S. Chung, K. J. Curran, J. E. Day, C. M. Dehnhardt, K. Dower, S. E. Drozda, R. K. Frisbie, L. K. Gavrin, J. A. Goldberg, S. Han, M. Hegen, D. Hepworth, H. R. Hope, S. Kamtekar, I.C. Kilty, A. Lee, L.-L. Lin, F. E. Lovering, M. D. Lowe, J. P. Mathias, H. M. Morgan, E. A. Murphy, N. Papaioannou, A. Pathy, B. S. Pierce, V. R. Rao, E. Saiah, I. J. Samardjiev, B. M. Samas, M. W. Shen, J. H. Shin, H. H. Soutter, J. W. Strohbach, P. T. Symanowicz, J. R. Thomason, J. D. Trzupek, R. Vagas, F. Vincent, J. Yan, C. W. Zapf, S. W. Wright, *J. Med. Chem*. **2017**, *60*, 5521–5542.
[23] S. Maramai, S. Gemma, S. Brogi, G. Campiani, S. Butini, H. Stark, M. Brindisi, *Front. Neurosci.* **2016**, *10*, 451e.
[24] J. Nunes, A. Grant McGonagle, J. Eden, G. Kiritharan, M. Touzet, X. Lewell, J. Emery, H. Eidam, J. D. Harling, N. A. Anderson, *ACS Med. Chem. Lett.* **2019**, *10*, 1081–1085.
[25] E. Naydenova, N. Pencheva, J. Popova, N. Stoyanov, M. Lazarova, B. Aleksiev, *Farmaco*. **2002**, *57*,189–194.
[26] H. Suzuki, M. B. B. Kneller, D. A. Rock, J. P. Jones, W. F. Trager, A. E. Rettie, *Arch. Biochem. Biophys*. **2004**, *429*, 1–15.
[27] G. M. Sheldrick, SHELXT – Integrated space-group and crystal-structure determination, *Acta Crystallogr. Sect. A: Found. Adv.* **2015**, *71*, 3–8.
[28] G. M. Sheldrick, Crystal structure refinement with SHELXL, *Acta Crystallogr. Sect. C: Cryst. Struct.* **2015**, *71*, 3–8.
[29] L. J. Farugia, WinGX and ORTEP for Windows: an update, *J. Appl. Crystallogr*. **2012**, *45*, 849–854.
[30] M. J. Frisch, G. W. Trucks, H. B. Schlegel, G. E. Scuseria, M. A. Robb, J. R. Cheeseman, G. Scalmani, V. Barone, B. Mennucci, G. A. Petersson, H. Nakatsuji, M. Caricato, X. Li, H. P. Hratchian, A. F. Izmaylov, J. Bloino, G. Zheng, J. L. Sonnenberg, M. Hada, M. Ehara, K. Toyota, R. Fukuda, J. Hasegawa, M. Ishida, T. Nakajima, Y. Honda, O. Kitao, H. Nakai, T. Vreven, J. A. Montgomery Jr., J. E. Peralta, F. Ogliaro, M. Bearpark, J. J. Heyd, E. Brothers, K. N. Kudin, V. N. Staroverov, R. Kobayashi, J. Normand, K. Raghavachari, A. Rendell, J. C. Burant, S. S. Iyengar, J. Tomasi, M. Cossi, N. Rega, N. J. Millam, M. Klene, E. J. Knox, J. B. Cross, V. Bakken, C. Adamo, J. Jaramillo, R. Gomperts, R. E. Stratmann, O. Yazyev, A. J. Austin, R. Cammi, C. Pomelli, J. W. Ochterski, R. L. Martin, K. Morokuma, V. G. Zakrzewski, G. A. Voth, P. Salvador, J. J. Dannenberg, S. Dapprich, A. D. Daniels, Ö . Farkas, J. B. Foresman, J. V. Ortiz, J. Cioslowski, D. J. Fox, Gaussian09; Gaussian, Inc.: Wallingford, CT, 2009.
[31] S. F. Boys, F. Bernardi, *Mol. Phys*. **1970**, *19*, 553–556.
[32] I. J. Bruno, J. C. Cole, P. R. Edgington, M. Kessler, C. F. Macrae, P. Mc Cabe, J. Pearson, J. Taylor, *Acta Crystallogr., Sect. B: Struct. Sci. Cryst. Eng. Mater*. **2002**, *58*, 389–397.
[33] O. Trott, A. J. Olson, *J. Comput. Chem*. **2010**, *31*, 455–461.
[34] H. M. Berman, J. Westbrook, Z. Feng, G. Gilliland, T. N. Bhat, H. Weissig, I. N. Shindyalov, P. E. Bourne, *Nucleic Acids Res.* **2002**, *28*, 235–242.
[35] Dassault Systèmes BIOVIA, Discovery Studio Modeling Environment, Release 2017, San Diego: Dassault Systèmes, 2016.

## Entry for the Table of Contents

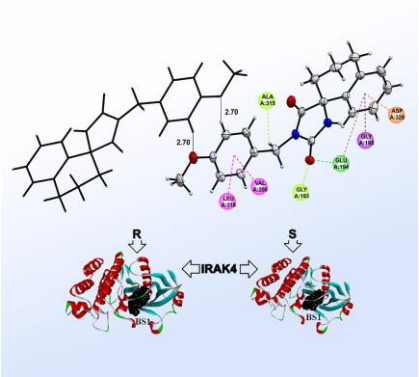


Development of the crystal structure of a newly synthesized spirohydantoin was described through interplay of homo and hetrerochiral dimeric motifs associated with different intermolecular interactions. A larger number of the contact fragments found in the environment of the tetralin unit within the crystal structure results from its larger contact surface, while the 4-methoxybenzyl unit provides a slightly greater contribution to the overall stabilization. This compound was further identified as a potential inhibitor of Kinase enzymes and AG protein-coupled receptors.